Influence of the Interface and Fiber Spacing on the Fracture Behavior of Glass Matrix Composites

by T. E. Matikas,* P. Karpur,* R. Dutton,† and R. Kim*

Abstract

In this work, a nondestructive methodology is provided to determine) presence of microcracking in unidirectional SiC fiber reinforced brittle (or ~ilicate glass) matrix composites and to detect internal cracks in the c\ sites that did not reach the surface of the specimen. The methodology is based on a combination of several ultrasonic techniques including shear back reflectivity (SBR), back-reflected surface wave imaging and acoustic microscopy. The composites used in this study were made with controlled fiber spacing consisting of regular arrays of either TiB₂ coated SIGMA 1240 or carbon coated SCS-6 monofilament fibers in a series of borosilicate glasses. The combinations of different constituents provided composite samples with various fiber matrix interface properties. The composites were subjected to axial loading, and the stress in the composite when matrix cracking first occurs was determined and compared with theoretical values provided by a semi-empirical model which can assume either a completely bonded (i. e. perfect) or completely unbonded (i. e. pure slip) fiber-matrix interface. Results from the tensile data for different glass matrix composite systems were also compared with data of interface elastic property evaluation using ultrasonic SBR technique, allowing investigation of the influence of the fiber-matrix interface elastic property, the volume fraction of the fibers, and the state of radial residual stresses at the interface, on the fracture behavior of glass matrix composites.

Keywords: ceramics, composite materials, fracture mechanics, glass matrix ceramic composites, microcracks, micromechanics, nondestructive characterization, ultrasound.

INTRODUCTION

The initiation of matrix microcracking in brittle matrix composites has been studied by several researchers in the past. The classic ACK model (Aveston et al., 1973) provides an energy criterion for the propagation of a "steady state crack" in a fiber reinforced composite. Recent work (Barsoum et al., 1992) observed that there is a relationship between the initiation of a matrix crack and the local fiber spacing.

Recent analytical and experimental work (Kaw and Pagano, 1993; Kim and Pagano, 1991; Pagano and Brown, 1993; Pagano and Kim, 1994 and 1995) with glass-ceramic composites containing Nicalon fibers in a calcium-aluminosilicate (CAS) matrix has supplied evidence that the increase in crack growth resistance noted in regions of high fiber volume fraction implies higher microcrack initiation stress levels for composites with uniformly and closely spaced fibers. An axisymmetric concentric cylinder model was used (Pagano and Brown, 1993) to describe the so-called "full cell cracking mode" which is a local fiber-bridging mode.

More recently, the matrix crack initiation process was characterized by the observation of the progression of fracture in unidirectional Nicalon-glass ceramic composites (Pagano and Kim, 1994 and 1995), and a semi-empirical model of the full cell cracking mode was developed to approximate the matrix cracking stress under a monotonically increasing axial tensile stress.

The objective of this work is to characterize, nondestructively, the fiber-matrix interface elastic behavior of unidirectional borosilicate glass/SiC fiber composites with controlled fiber spacing. Further, the effects of various interface properties as well as residual stresses are assessed using the ultrasonic SBR technique. The influence of the interface on the composite cracking stress (CCS, defined as the applied composite stress at which matrix cracking first occurs) is also studied by assessing the initiation of matrix microcracking under axial mechanical loading.

Elasticity Model

The semi-empirical model (Pagano and Kim, 1994, 1995) was used to calculate the matrix axial stress for which microcracking initiates in the matrix. The basis of this model is illustrated in Figure 1 and shows that regions with higher local fiber volume fraction provide higher matrix cracking stress, σ_M (MCS, defined as the stress in the matrix at crack initiation).

The plot in Figure 1 presents the average values of pre-cracked matrix stress, σ_M, versus average fiber spacing, s, for a CAS glass ceramic composite with 40 percent Nicalon fibers after a series of incremental loading in both tension and flexure (Pagano and Kim, 1995). The curve in the solid line in Figure 1 derived from the equation of the semi-empirical model:

$$(1) \qquad 2\sigma_m \left[\frac{a+s}{\pi} \right]^{1/2} = K_{IC}$$

where a is the fiber radius and K_{IC} is the matrix fracture toughness (1.84 MPa√m for Nicalon/CAS composite). Equation 1 represents the relationship between the local fiber spacing and the crack initiation stress, and was developed by computing (Pagano and Brown, 1993) the average stress in the matrix, σ_M, when each crack initiates using a four-phase concentric cylinder model as shown in Figure 2.

Calculation of the Composite Cracking Stress

In order to compare the experimental results with the predictions of the model, the matrix cracking stress, σ_M, obtained from the semi-empirical model must be converted to a composite cracking stress, σ_C, (Dutton, Pagano, Kim, submitted for publication). There are two limiting cases for the value σ_C depending upon the assumed fiber-matrix interface properties:

* Research Institute, University of Dayton, 300 College Park Ave., Dayton OH 45469-0127; (513) 255-9808; fax (513) 255-1363; e-mail: matikat@ml.wpafb.af.mil.
† National Institute of Standards and Technology, Wright Laboratory, Materials Directorate, WL/MLLN, Wright-Patterson AFB, OH 45433-7817.
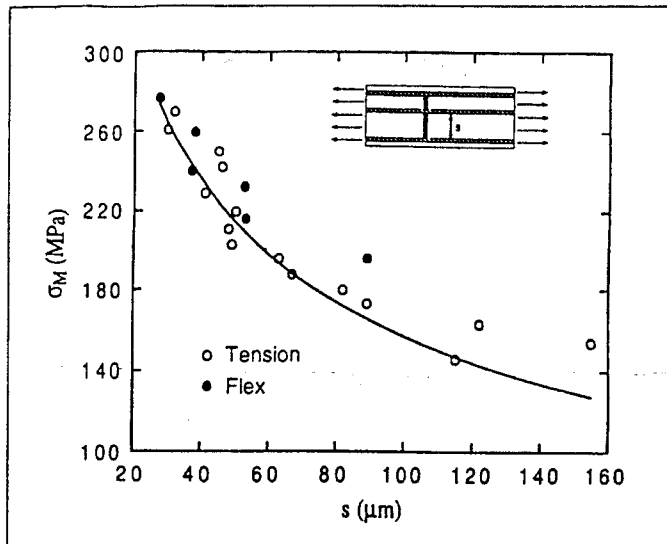
Figure 1 — Semiempirical model for the evaluation of fracture behavior of uniaxial ceramic matrix composites with variable fiber spacing.

■ A continuous interface with complete load transfer from the matrix to the fiber.

■ A sliding interface with no friction, in which no load is transferred from the matrix to the fibers.

The composite matrix stress assuming a continuous interface was determined using the concentric cylinder model, NDSANDS (Pagano, Tandon, 1988), to calculate the axial stress in the matrix due to thermal loading, σ_z^m (T) (i.e. $\Delta T = 500$ °C [932 °F] and $\sigma_C = 0$ MPa), and the matrix stress under a unit uniaxial composite stress with no thermal load, σ_z^m (S) (i.e. $\Delta T = 0$ °C [32 °F] and $\sigma_C = 1$ MPa), which represents the percentage of the composite stress carried by the matrix. The composite cracking stress is then given by the expression

$$
(2) \qquad \sigma_c = \frac{\sigma_m - \sigma_z^m(T)}{\sigma_z^m(S)}
$$

The composite matrix stress assuming a sliding frictionless interface is given by

$$
(3) \qquad \sigma_C = (1 - v_f)\, \sigma_M
$$

where, in both cases, σ_M is given by the expression

$$
(4) \qquad \sigma_m = \frac{K_{IC}}{2} \sqrt{\frac{\pi}{a+s}}
$$

and v_f is the volume fraction of fibers in the composite, $v_f = a^2/b^2$, which is used to calculate the required uniform fiber spacing, $s = 2(a - b)$.

Experimental Procedure

The composite cracking stress of the ceramic composite samples was evaluated using incremental loading (load/listen/look). Fiber volume fractions were determined using the rule of mixtures with the moduli of the respective fibers and matrix determined from separate tests. Axial and transverse strains were measured using strain gages. Free edges and flat surfaces of specimens were polished with diamond paste in order to enhance microscopic imaging for crack detection. The upper and lower surfaces were coated with a thin layer of epoxy to reduce the dominance of surface flaws. Acoustic emission and photomicrographic techniques were employed for detection of initial matrix cracking. Photomicrographic analysis was mainly used to verify the acoustic emission results through physical observation of cracks. Additional information on
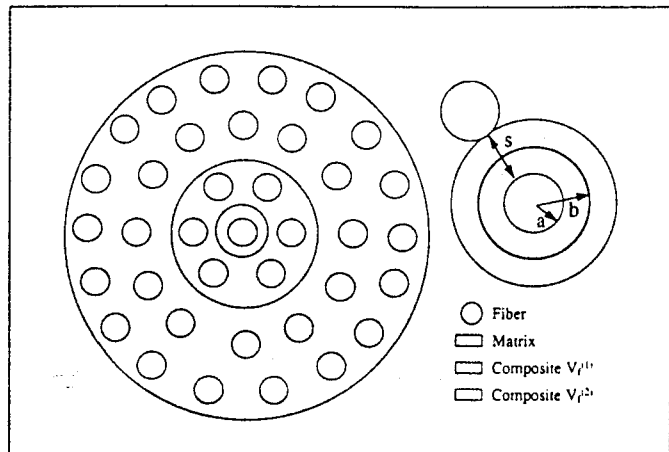

Figure 2 — Four-phase concentric cylinder model to account variable fiber spacing in an hexagonal array.

the experiments can be found in the literature (Dutton et al., in process; Pagano and Kim, 1995). Ultrasonic techniques were used to detect the presence of surface cracks and internal cracks, and to image the interface debonding due to microcracking and are reported in this paper.

Sample Fabrication

Different borosilicate glasses were used in this study, including 7040 glass and two custom glasses named "E" and "F" which were supplied by Corning (average size ~8 µm), with varying K_2O/B_2O_3 ratios (Jero et al., 1991). The glass compositions were graded in order to essentially vary the thermal expansion coefficient of the glass while the elastic properties remained the same. Therefore, because of the mismatch in the thermal expansion coefficients between the different types of glasses and the fibers, the resulting residual radial thermal stresses at the interface after processing vary from tensile to compressive. Two different types of fibers were utilized in the study. One wa a TiB₂ coated SIGMA 1240 fiber with a diameter of 102 µm and the other a carbon coated SCS-6 SiC fiber with a diameter of 142 µm. The borosilicate glass strongly wets the TiB₂ coating of the SIGMA 1240 fiber but weakly wets the carbon coating of the SCS-6 fiber. This allowed the investigation of the effects of bonding at the fiber-matrix interface on the initiation of matrix microcracking.

The glasses were tape cast into green tapes with a relative density of ~50 percent. The green tapes were then cut into coupons and laminated onto fiber mats with the desired regular fiber spacing (27 or 48 fibers per cm). The volume fraction of fibers in the composites was varied by altering the thickness of the green tape and using the two different fiber spacings. After lamination the composites were inserted into a tube furnace and vacuum sintered at 710 °C (1,310 °F) for one hour. The samples were then hot isostatically pressed at 650 °C (1,202 °F) for 30 min with an applied pressure of 35 MPa to remove any residual porosity (< 2 percent). The resulting samples were approximately 100 mm long by 20 mm wide (4 in. long by 0.78 in. wide) with a thickness of 2 mm (0.78 in.) (Gustafson et al., in press).

Detection of Matrix Microcracking and Interface Debonding Using Ultrasonic Techniques

Following mechanical testing, the specimens were ultrasonically evaluated to determine the initiation and accumulation of surface as well as internal cracks, and also to assess the interfacial debonding due to matrix microcracking. Several ultrasonic techniques were used in this work:

■ Scanning acoustic microscopy (SAM) (Blatt et al., 1993; and Karpur et al., 1995) at 50 MHz was performed on the specimens to investigate the damage accumulation in the matrix as well as the interface integrity after mechanical testing. The principle of operation of a SAM transducer is based on the production and propagation of surface acoustic waves (SAW) as a direct result of a combination of

the high curvature of the focusing lens of the transducer and the defocus of the transducer into the sample. The contrast of the images obtained using SAM is based on the attenuation and reflection of SAW. In addition, the sensitivity of the SAW signals to the surface and subsurface features depends on the degree of defocus.

The defocus distance also has another important effect on the SAW signal obtained by the SAM transducer: the degree of defocus dictates whether the SAW signal is well separated from the specular reflection or interferes with it. Thus, depending on the defocus, the SAM technique can be used either to map the interference phenomenon in the first layer of subsurface fibers or to map the surface and subsurface features in the sample. Figure 3 shows a SAM image of a SIGMA 1240/7040 unidirectional composite subjected to tensile loading. Many matrix cracks are shown in the image perpendicular to the direction of the fibers. From the SAM image it appears that there is not extensive interface debonding as a result of the matrix cracking. That is, only localized interface debonding occurs in the neighborhood of the cracks.
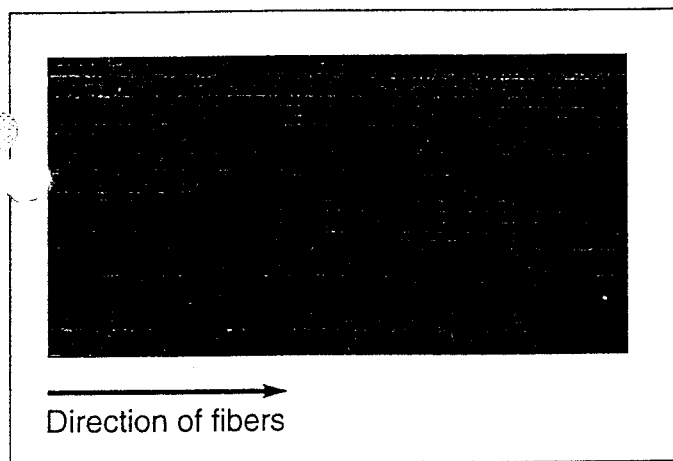

Figure 3 — Unidirectional SIGMA 1240-7040 composite sample. Scanning acoustic microscopy image showing matrix microcracking and fiber-matrix interface debond limited to the proximity of the matrix cracks.

This localized debonding behavior of the interface in the case of a SIGMA 1240/7040 composite system indicates a strong interfacial bonding compared to the weak interfacial bond of an SCS-6/7040 composite shown in Figure 4. Figure 4a shows an acoustic microscopy image from a SCS-6/7040 unidirectional composite sample wherein several surface cracks are observed as well as extended fiber-matrix interface debond (the cracks are perpendicular to the direction of the fibers as shown in Figure 4a). These indications about the interfacial bonding were also confirmed by ultrasonic evaluation of the fiber-matrix interface using SBR technique as described in a later section of this paper. The above results were consistent with the fact that the borosilicate glass strongly wets the TiB$_2$ coating of the SIGMA 1240 fibers providing stronger interfacial bonding, and weakly wets the carbon coating of the SCS-6 fiber providing weak interfacial bonding.

■ Surface acoustic wave (SAW) immersion imaging was implemented to detect the surface cracks alone. An ultrasonic transducer operating at 25 MHz in a pulse-echo mode was used in this study. The ultrasonic beam was incident on the surface of the specimen at the Rayleigh angle and in the plane of the fibers (perpendicular to the cracks). The sample was scanned and the reflection from the cracks was gated to image surface cracks alone. Figure 4b shows the surface wave image from the same SCS-6/7040 composite sample as discussed before. Only the surface cracks were detected using this technique and correspond one to one to the cracks also detected using acoustic microscopy (Figure 4a) as indicated by the arrows.

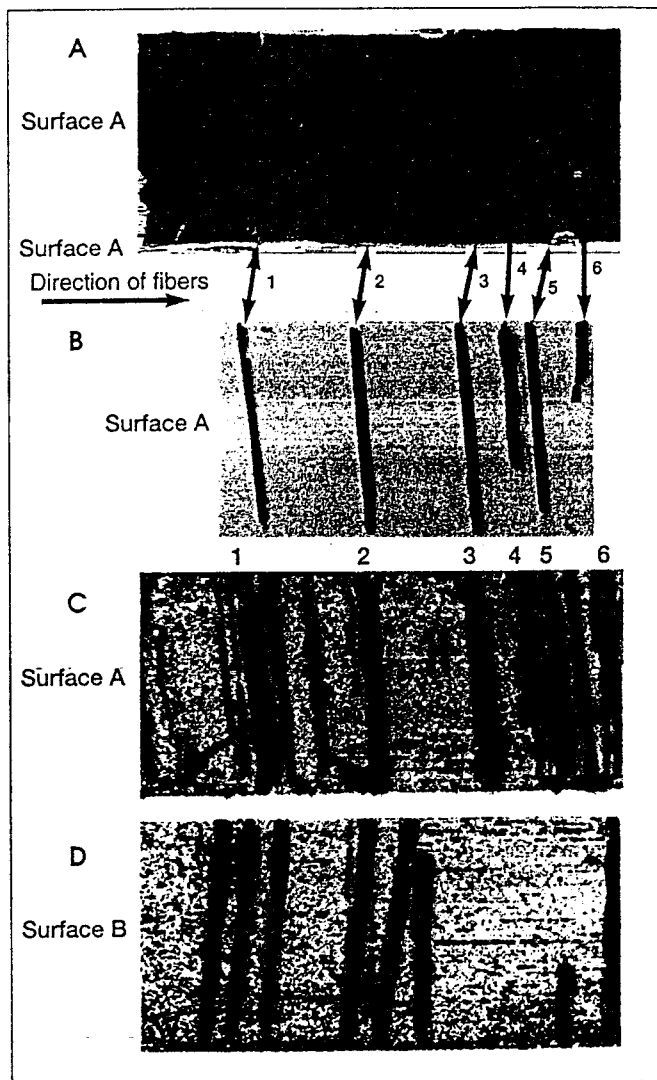■ Finally, a 25 MHz SBR technique (Karpur, et al., 1995; Matikas

Figure 4 — Unidirectional SCS-6-7040 composite sample. (a) Scanning acoustic microscopy image of the surface A of the composite sample showing surface cracks and extensive fiber matrix interface debond due to matrix microcracking (the surface cracks are indicated by numbers). (b) Surface wave image of the surface A of the composite sample obtained when second reflection of surface acoustic waves was monitored for mapping. The image shows surface cracks alone (the corresponding cracks in SAM and SAW images are indicated by arrows). (c) Shear wave back reflectivity image of the surface A of the composite sample showing the presence of internal cracks in addition to the surface cracks. Both surfaces of the composite sample were imaged and by comparing the surface A and surface B, the matrix microcracks that are completely inside the composite panel and did not reach either surface of the sample were detected. (d) SBR image of the surface B of the composite sample.

and Karpur, 1992 and 1993a) was used to detect the presence of internal cracks in addition to cracks that reached the surface of the specimen. In this case, oblique incidence shear waves (incidence of the ultrasonic beam between the first and the second critical angles of the glass matrix material) in the plane of the fibers were reflected from the cracks back to the transducer. Figure 4c shows the SBR image of the SCS-6/7040 composite sample (same surface as in Figures 4a and 4b). The six surface cracks can be observed in this image producing stronger back-reflection than several internal cracks. The crack numbered 6 starts at the surface in one side of the sample and propagates internally to the other side. Similarly for the crack numbered 4. Cracks 1 and 2 are connected to internal cracks with microcracks at 45 degrees to the fiber axis. Figure 4d shows the

back surface (labeled B) of the same composite sample. By comparing Figures 4c and 4d, the existence of completely internal cracks that did not reach either surface A or B of the composite (full cell cracks) can be demonstrated.

The ultrasonic methodology described above is shown to be effective in detecting the presence of new microcracks in brittle matrix composites when it is used to image composite samples after each cycle of the mechanical tests. Therefore, the technique can be used to detect initiation events in a composite and to obtain an accurate plot of the number of new cracks versus load.

Ultrasonic Characterization of the Fiber-Matrix Interface Region

Shear-wave back reflectivity technique at 25 MHz was used to image and quantify the stiffness of the fiber/matrix interface region for both SIGMA 1240 and SCS-6 fibers embedded in 7040 glass as well as in glass E and glass F. The technique consists of interrogating the interface with an ultrasonic beam incident on the specimen between the first and second critical angles of the matrix so that only mode converted shear waves are incident on the fiber perpen-:':ular to its circumference, as shown in Figure 5. A theoretical del (Matikas and Karpur, 1993a) was developed which aids in th termination of various experimental parameters such as the fre ncy of ultrasound and angle of incidence while providing the relationships necessary to interpret the experimental results. The theoretical model considers the reflection of an ultrasonic wave front from fibers embedded in a matrix. For the development of the theoretical model, the interface between the matrix and the fiber is modeled by assuming continuity of normal and shear stresses and normal displacements at the interface, and by allowing the discontinuity of shear displacements at the interface. It is assumed that the vibration is transmitted instantaneously from one medium to the other by weightless shear springs with an equivalent rigidity of N_s (MPa/μm), which defines the shear stiffness coefficient of the interface. Accordingly, the interface conditions are:

$$\{\sigma^P\} = 0$$

$$\{\sigma^T\} = 0$$

$$\{u^P\} = 0$$

$$\sigma^T = N_S \bullet [u^T]$$

. ..ere the superscripts P and T denote the normal and tangential

displacements/stresses respectively; the brackets denote the jump of a function across the interface, and the braces denote the vectorial resultant of stresses at the interface. In this study, the above model has been used to assess the interfacial properties in several composite systems. In this analysis, the ultrasonic beam is considered to be incident on the composite such that the refracted wave is always normal to the fiber circumference (Figure 5). The angle of incidence is such that the refracted shear waves are incident on the fibers and reflected back to the transducer. The reflection can be quantified by the shear back-reflection coefficient (SBRC) from the fiber as shown in Equation 4. This can be calculated after solving the wave equation using the boundary conditions described previously:

$$(4) \qquad SBRC = T_M R_F T_W$$

where the terms on the right hand side of the equation are functions of the properties of the matrix and the fiber, the diameter of the fiber, the angle of incidence, the ultrasonic frequency of interrogation, and the interfacial shear stiffness coefficient (N_S) which is the amount of elastic shear stress transferred through the interface per unit of relative displacement, and represents the ratio of shear modulus of the interphase material and the thickness of the interphase region (Karpur et al., 1995).

An example of the theoretical relationship between the ultrasonic back-reflection coefficient and shear property of the interface region for an ultrasonic frequency of interrogation of 25 MHz is obtained from the model (Matikas and Karpur (1993a) and is illustrated in Figure 6 for two composite systems: SIGMA 1240-glass E and SCS-6-glass E. Similar theoretical curves were obtained for SCS-6 and SIGMA 1240 fibers embedded in 7040 and F glasses.

Figure 7 shows the ultrasonic images of two different glass ceramic composites as fabricated (prior to any mechanical testing) obtained using the SBR technique at 25 MHz and with an angle of incidence of 19 degrees (Matikas et al., submitted for publication). Figure 7a shows the image of a SIGMA 1240-glass E composite where the interface is uniformly formed due to the fact that the glass strongly wets the fiber. Figure 7b shows the image of a SCS-6-glass E composite. In this case, partial interface debonding is observed because the glass weakly wets the fiber.

The details on the experimental procedure for the measurement of the interfacial stiffness (Matikas and Karpur, 1993b) are summarized below. The ultrasonic signal back-reflected from the fiber is first digitized. A reference signal is then obtained from a reference block made from the matrix material. The reference block is fabricated with a specific geometry so that if the ultrasonic beam is

Figure 5 — Configuration of the shear back reflectivity technique used for fiber-matrix interface evaluation.
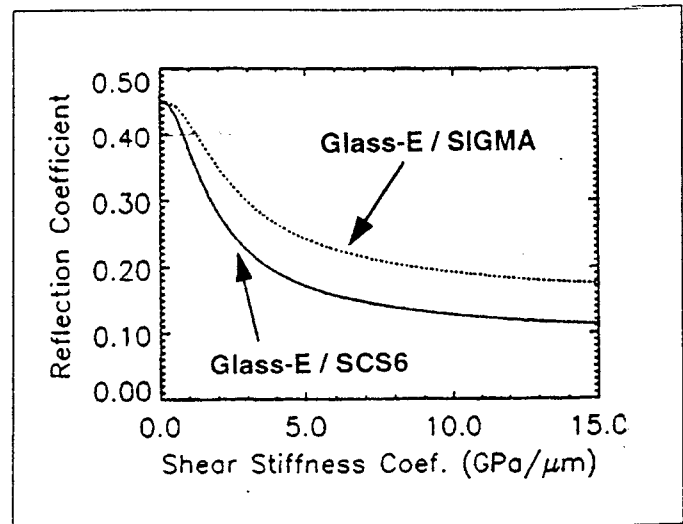

Figure 6 — Amplitude of the back-reflection coefficient at 25 MHz versus interface shear stiffness coefficient for two different composite systems made with the same matrix material (glass E) and different fibers (SCS-6 and SIGMA 1240).

incident on its surface with the same angle of incidence that was used to interrogate the embedded fiber in the composite, the beam is perpendicular to one side of the block which is sealed with air. Therefore, the back reflected signal from the reference block contains the total reflection from a path in the matrix material of similar length. The ratio of the signal from the fiber and the reference in the Fourier domain at a specific frequency (25 MHz was selected in this case based on information obtained from the analysis [Matikas and Karpur, 1993a]) gives a direct measurement of the reflection coefficient. The interface shear stiffness coefficient is then obtained using the theoretical curves shown in Figure 6, and the results are tabulated in Table 1.

Table 1 Values of the interface shear stiffness coefficients obtained from experimentally measured back-reflection coefficients for six different glass ceramic composites

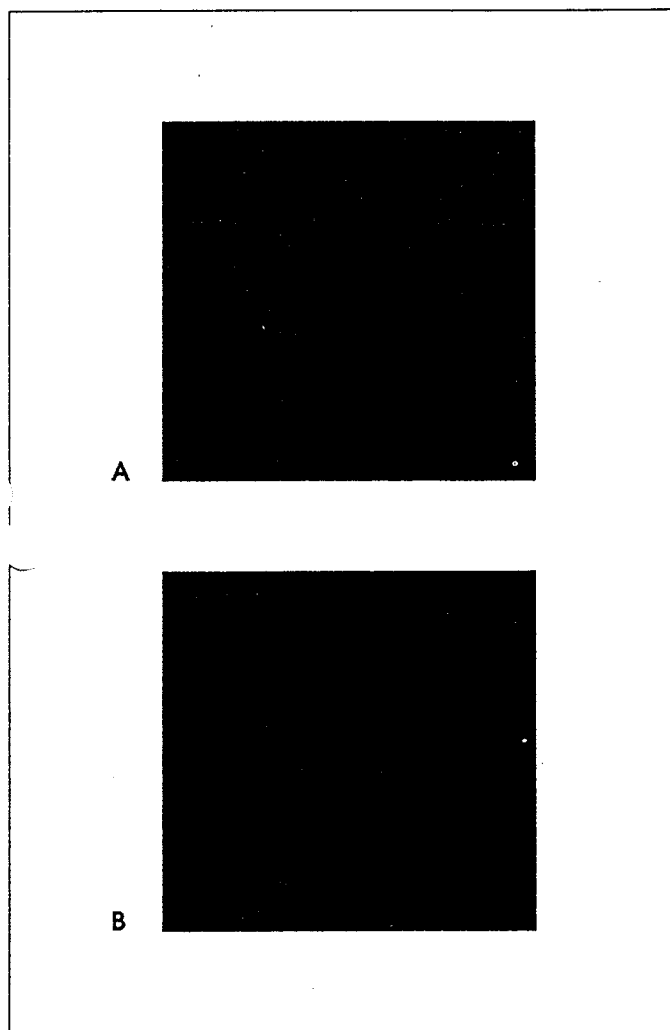| Composite system	Reflection coefficient	Shear stiffness coefficient (MPa/μm)
SIGMA-7040	0.390	812 ± 19
SIGMA-F	0.383	815 ± 18
SIGMA-E	0.442	368 ± 127
SCS-6-7040	0.423	483 ± 36
SCS-6-F	0.439	293 ± 45
SCS-6-E	0.448	211 ± 166

Figure 7 — Ultrasonic shear back reflectivity imaging showing (a) a uniform interface in the case of a SIGMA 1240-Glass-E composite, and (b) a partially debonded interface in the case of a SCS-6-Glass-E composite.

As can be seen from Table 1, the experimental results for the interfacial stiffness of the various composite systems indicate that since SIGMA/7040 and SIGMA/F composites have compressive radial residual stresses at the interface and the glass matrix strongly wets the fiber coating, the interface has a higher value of stiffness coefficient. In the case of these composites, the ultrasonic back reflection coefficient was found to be uniform along the length of the fibers, i.e., the data scatter in the ultrasonically measured interfacial stiffness was very small as shown in Table 1 and Figure 8. Scatter in ultrasonically measured interfacial stiffness means that the back-reflected ultrasonic amplitude (which is used to determine the interfacial shear stiffness coefficient) varies from point to point along the length of the fiber and is an indication of the lack of uniformity of the interface along the length of the fiber. Also, the fiber-matrix interface in the case of a SIGMA-E composite (tensile radial residual stress) has lower interfacial shear stiffness compared to SIGMA-7040 and SIGMA-F composites. In this case the scatter in the ultrasonically measured interface stiffness was high as shown in Figure 8 indicating the possibility of partial interface debonding. Further, SCS-6 reinforced glass matrix (7040, E or F) composites (glasses do not strongly wet the carbon coating of the SCS-6 fiber) have low values of interfacial shear stiffness coefficient. In the case of SCS-6-F and SCS-6-7040 composites the interface was uniform and the scatter in the ultrasonically measured interfacial shear stiffness was low compared to the data high scatter of the SCS-6-E composite (Figure 8).

The nondestructive evaluation of the fiber-matrix interface can be summarized as follows: SIGMA-7040, SIGMA-F, SCS-6-F, and SCS-6-7040 composites have a continuous interface, SIGMA-E and SCS-6-E composites have possible partial debonding. The fiber-matrix interface in the case of SIGMA-7040 and SIGMA-F composites was found to be stiffer than in the case of SCS-6-F, SCS-6-7040 composites. These observations were compared with experimental results of the composite cracking stress as discussed in the following section.

Experimental Results on the Composite Cracking Stress

The composite cracking stress was measured for a variety of glass ceramic composites made with SIGMA 1240 and SCS-6 fibers. The material properties of the constituents of the composites used in this study are shown in Table 2. Due to the mismatch in thermal expansion coefficients, α, given in Table 2 for the different composite constituents, the calculated precrack radial stresses at the fiber-matrix interface range from compressive for the composites with 7040 glass matrix (~ –17 MPa), almost zero for the F glass (~ –0.3 MPa), to tensile for the E glass (~ 5 MPa). The experimental results for the composite cracking stress and model predictions are presented in Table 3 and plotted in Figures 9a and 9b.
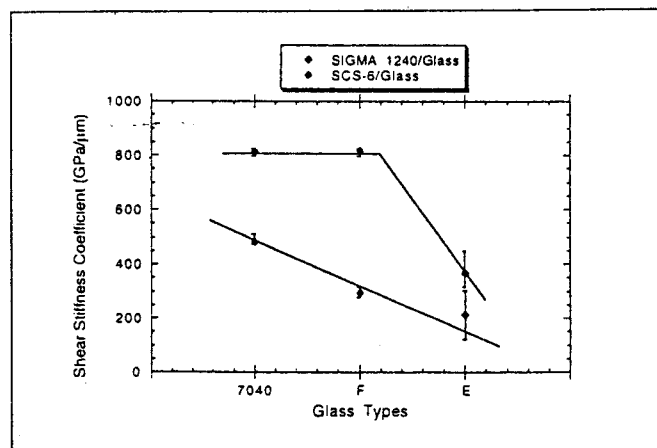

Figure 8—The interfacial shear stiffness coefficient (N_S) for the various glass ceramic matrix composites. The error bars indicate the scatter in the measurement of N_S along the length of the fibers embedded in the glass matrix.

Table 2 Material properties

	Glass		
	7040	E	F
E (GPa)	50	58	58
υ	0.20	0.20	0.20
α (× 10^{-6}/°C)	5.40	3.95	4.25
K_{IC} (MPa√m)	0.77	0.77	0.77
ρ (g/cm³)	2.24	2.21	2.26

	Fibers	
	SIGMA 1240	SCS-6
E (GPa)	325	390
υ	0.20	0.20
α (× 10^{-6}/°C)	4.23	4.23
Diameter (μm)	102	142
ρ (g/cm³)	3.65	3.17

Figures 9a and 9b illustrate the results from Table 3 for the SIGMA 1240 and SCS-6 fibers in the borosilicate glass matrices. The semiempirical model assumes two bounds:
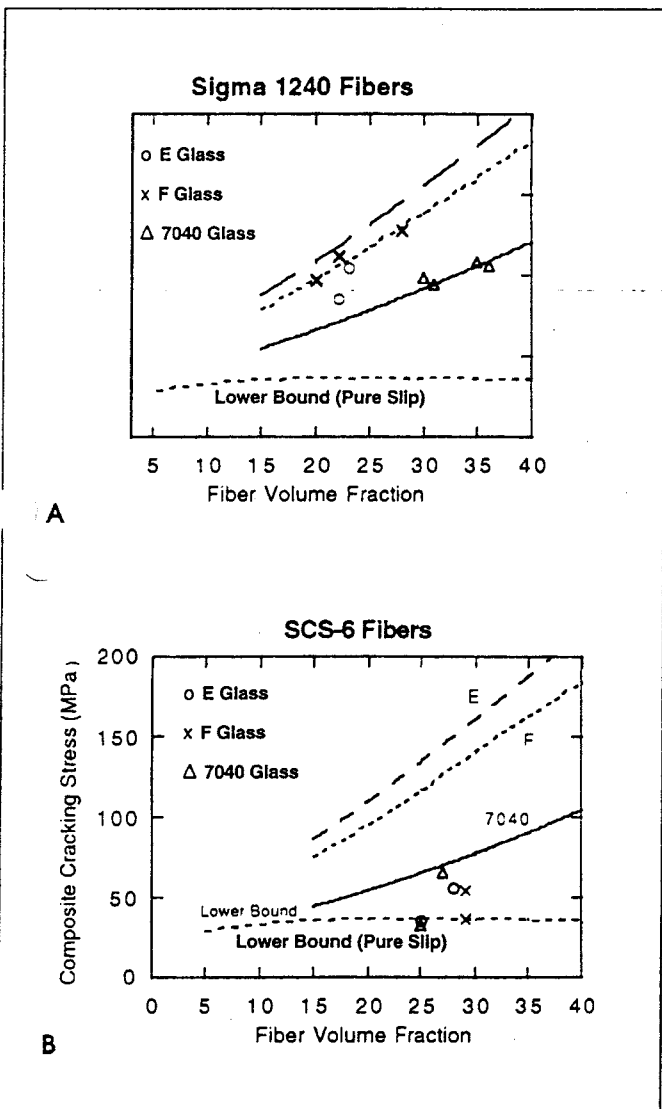
A

B

Figure 9 — Model and experimental results for (a) SIGMA 1240 fibers, and (b) SCS-6 fibers. The lower bound in the theoretical curves indicates pure slip.

- An upper bound showing the matrix cracking stress when there is a perfect interface between the matrix and the fiber and if no residual stresses were present after processing.
- A lower bound where there is no bonding between the matrix and the fiber.

As can be seen, the effect of residual thermal stresses due to processing is to lower the level of stress at which initial matrix cracking occurs in the glass matrix.

Table 3 and Figure 9a show that the semi-empirical model with a continuous interface agrees well with the experimental results for the 7040 and F glasses (compressive radial residual stress) but overestimates the E glass (tensile radial residual stress). Table 3 and Figure 9b show that most of the experimental data are close to the lower bound model prediction with a sliding frictionless interface (i.e. debonded interface). This is because the borosilicate glasses do not strongly wet the carbon coating of the SCS-6 fibers, therefore, the fiber-matrix interface is relatively weak, possibly allowing interfacial slip to occur.

The nondestructive evaluation of the interfacial stiffness is in agreement with the experimental results as discussed in the previous section.

Table 3 Predictions on the composite cracking stress (CCS) using the semiempirical model of full cell cracking mode and experimental data

Glass Matrix	SIGMA 1240 fibers		
	V_f (%)	CCS (MPa) experiment	CCS (MPa) Pure slip-perfect bond
7040	30	98	41/91
	35	107	40/105
	36	105	40/108
F	20	97	41/98
	22	112	41/106
	28	128	41/130
E	22	85	41/117
	23	104	41/122

Glass Matrix	SCS-6 fibers		
	V_f (%)	CCS (MPa) experiment	CCS (MPa) Pure slip-perfect bond
7040	25	32	35/65
	27	65	35/70
F	29	54	36/136
E	25	35	35/133
	28	55	35/149

Conclusion

In this paper, an ultrasonic nondestructive methodology has been presented and shown to be effective for detection of the presence of microcracking and for monitoring of damage accumulation in glass matrix ceramic composites. Further, the methodology provides imaging of internal matrix cracks in addition to surface cracks, and also can detect fiber-matrix interface debonding in a precrack mode as well as after matrix microcracking occurs. Another ultrasonic nondestructive technique has also been presented for the characterization of the fiber-matrix interface elastic behavior through the quantification of a parameter so-called the "interface shear stiffness coefficient." From the results presented in this paper, it can be concluded that there is a strong correlation between predictions of the semiempirical model, experimentally measured composite cracking stress (which is a measurement of the fracture behavior of the composites) for various glass matrix composites

with variable fiber volume fraction and interface properties, and the ultrasonically characterized interface elastic behavior.

Acknowledgments

References

Aveston, J., G. Cooper, and A. Kelly, "Single and Multiple Fracture," *The Properties of Fiber Composites*, Conference Proceedings NPL, 1973, p 15. IPL, Guildford, UK.

Barsoum, M., P. Kangutkar, and A.S.D. Wang, "Matrix Crack Initiation in Ceramic Matrix Composites. Part I: Experiment and Test Results," *Composites Science and Technology*, Vol. 43, No. 3, 1992, pp 257–270.

Blatt, D., P. Karpur, D.A. Stubbs, and T.E. Matikas, "Observations of Interfacial Damage in the Fiber Bridged Zone of a Titanium Matrix Composite," *Scripta Metallurgica et Materialia*, Vol. 29, 1993, pp 851–856.

Dutton, R.E., N.J. Pagano, and R.Y. Kim, "Crack Initiation in Borosilicate Glass-SiC Fiber Composites," *Journal of the American Ceramics Society*, in process.

Gustafson, C.M., R.E. Dutton, and R.J. Kerans, "Fabrication of Glass Matrix Composites by Tape Casting," *Journal of the American Ceramics Society*, in press.

Jero, P.D., R.J. Kerans, and T.A. Parthasarathy, "Effect of Interfacial Roughness on the Frictional Stress Measured Using Push-out Tests," *Journal of the American Ceramics Society*, Vol. 74, No. 11, 1991, pp 2793–2801.

Karpur, P., T.E. Matikas, M.P. Blodgett, J.R. Jira, and D. Blatt, "Nondestructive Crack Size and Interfacial Degradation Evaluation in Metal Matrix Composites Using Ultrasonic Microscopy," *Special Applications and Advanced Techniques for Crack Size Determination*, ASTM STP 1251, ed. by J.J. Ruschau and J.K. Donald, 1995, pp 130–146. American Society for Testing and Materials, Philadelphia, PA.

Karpur, P., T.E. Matikas, and S. Krishnamurthy, "Ultrasonic Characterization of the Fiber-Matrix Interphase/Interface for Mechanics of Continuous Fiber Reinforced Metal Matrix and Ceramic Matrix Composites," *Composites Engineering*, Special Issue on Fiber-Matrix Interfaces, Vol. 5, No. 6, 1995, pp 697–711.

Kaw, A.K., and N.J. Pagano, "Axisymmetric Thermoelastic Response of a Composite Cylinder Containing an Annular Matrix Crack," *Journal of Composite Materials*, Vol. 27, No. 6, 1993.

Kim, R.Y., and N.J. Pagano, "Crack Initiation in Unidirectional Brittle-Matrix Composites," *Journal of the American Ceramics Society*, Vol. 74, No. 5, 1991, pp 1082–1090.

Matikas, T.E., and P. Karpur, "Matrix-Fiber Interface Characterization in Metal Matrix Composites Using Ultrasonic Shear-Wave Back-Reflection Coefficient Technique," *Review of Progress in Quantitative Nondestructive Evaluation*, Vol. 12B, ed. by D.O. Thompson and D.E. Chimenti, 1992, pp 1515–1522. Plenum Press.

Matikas, T.E., and P. Karpur, "Ultrasonic Reflectivity Technique for the Characterization of Fiber-Matrix Interface in Metal Matrix Composites," *Journal of Applied Physics*, Vol. 74, No. 1, 1993, pp 228–236 (1993a).

Matikas, T.E., and P. Karpur, "Micro-mechanics Approach to Characterize Interfaces in Metal and Ceramic Matrix Composites," *Review of Progress in Quantitative Nondestructive Evaluation*, Vol. 13B, ed. by D.O. Thompson and D.E. Chimenti, 1993, pp 1477–1484. Plenum Press (1993b).

Matikas, T.E., P. Karpur, S. Krishnamurthy, and R.E. Dutton, "A Nondestructive Approach to Correlate the Interfacial Defects Induced During Processing of MMCs and CMCs with the Consolidation Parameters," *JOM*, in process.

Pagano, N.J., and G.P. Tandon, "Elastic Response of Multi-directional Coated-fiber Composites," *Composites Science and Technology*, Vol. 31, 1988, pp 273–293.

Pagano, N.J., and H. W. Brown III, "The Full-cell Cracking Mode in Unidirectional Brittle-matrix Composites," *COMPOSITES*, Vol. 24, No. 2, 1993, pp 69–83.

Pagano, N.J., and R.Y. Kim, "Progressive Microcracking in Unidirectional Brittle Matrix Composites," *Mechanics of Composite Materials*, Vol. 1, No. 1, 1994, pp 3–29.

Pagano, N.J., and R.Y. Kim, "Progressive Fracture Modes in a Unidirectional Brittle Matrix Composite under Tension," paper presented at ASME Symposium on Composites, Santa Monica CA, 1995.